

# PROCEEDINGS OF SPIE

[SPIDigitalLibrary.org/conference-proceedings-of-spie](https://SPIDigitalLibrary.org/conference-proceedings-of-spie)

## Development and assessment of lidar modeling to retrieve IOPs

Strait, Christopher, Twardowski, Michael, Dalglish, Fraser, Tonizzo, Alberto, Vuorenkoski, Anni

Christopher Strait, Michael Twardowski, Fraser Dalglish, Alberto Tonizzo, Anni Vuorenkoski, "Development and assessment of lidar modeling to retrieve IOPs," Proc. SPIE 10631, Ocean Sensing and Monitoring X, 106310U (25 May 2018); doi: 10.1117/12.2309998

**SPIE.**

Event: SPIE Defense + Security, 2018, Orlando, Florida, United States

# Development and assessment of lidar modeling to retrieve IOPs

Christopher Strait, Michael Twardowski, Fraser Dalgleish, Alberto Tonizzo, and Anni Vuorenkoski

<sup>a</sup>Harbor Branch Oceanographic Institute at Florida Atlantic University, 5600 US 1 North, Fort Pierce, Florida 34946.

## ABSTRACT

A synthetic bio-optical dataset of inherent optical properties (IOPs) was created based on Chlorophyll concentrations ranging between 0.01 and 30 mg m<sup>-3</sup>. Dissolved and particulate fractions of absorption were varied to account for the natural ranges in values. The IOPs will then be used as inputs to a time-resolved Monte-Carlo radiative transfer model to generate accurate lidar backscatter time history wave forms. Test experiments were performed to validate the model, where the primary lidar geometry in the model matched an existing system developed at HBOI under NOAA-OAR funding. The system uses blue and green pulsed laser sources (473 and 532 nm, respectively) and has two telescopes arranged at a 10° offset (on and off axis) from one another. The field of view of the telescopes is set at 1°. Approaches are being investigated to invert simulated and measured lidar results to derive input water column IOP properties. Results are tested through application to lidar measurements collected in an experimental tank with known suspended particle type and concentration.

**Keywords:** Ocean sensing and monitoring, underwater imaging, remote sensing, inversion algorithms

## 1. INTRODUCTION

Inherent Optical Properties (IOPs) in the open ocean have shown a strong dependence on chlorophyll concentration. Contemporary empiricism of these relationships began with Morel<sup>1</sup> and was further formalized by Lee et al., in IOCCG synthetic data sets from 2006<sup>2</sup>. Currently, methods used to measure IOPs usually include a profiling package which has a very small sampling volumes<sup>15</sup>. This is a slow and ultimately intrusive process as particles are pumped into flow cells, altering their orientation and breaking living cells, adding ambiguity and error to the measurement. To better understand the distribution of chlorophyll concentration and other particles and their relation to the carbon cycle of the ocean, it is imperative that systems which can measure over great temporal and spatial scales be employed.

Combining autonomous platforms and lidar technologies can provide longer duration, lower cost and more efficient deployments, as well as the capability to profile the water column and explore regions where aerial and boat mounted systems cannot access. This also removes the need for correction of air water interface effects which typically manifest in large surface returns and potential losses due to surface roughness. Most oceanographic lidar systems use pulsed lasers rather than Continuous Wave (CW) lasers. Using a pulsed laser system has two main advantages over CW laser systems: (1) temporal gating of the return to reduce path backscatter and increase the signal-to-noise ratio and (2) time history of the backscattered return may also be inverted to determine bulk inherent optical properties as well as those of layers with ranges of up to tens of meters in clear waters<sup>3</sup>. Without the pulsed laser it is much more difficult to get more than a single averaged value of attenuation through the sample area.

At close range the receiving optics can detect only multiply scattered light, as there is no overlap of the laser and receiving optics. When these two cones overlap it begins the common volume. In relatively clear waters the peak of the common volume return occurs early within this intersection. At higher turbidities the loss of signal with distance will be greater, thus increasing the slope of the common volume portion of the lidar return and making the common volume peak indistinguishable.

The standard single scatter lidar formula follows this general form:

$$p(r) = C \frac{\beta_{\pi}(r)}{r^2} \exp \left[ -2 \int_0^r K_{\text{sys}}(r') dr' \right]$$

where the time resolved backscattered return signal (P) at a given distance (r) is a function of the output power of the laser, the geometric layout of the lidar system (source and receiver) and the optical properties of the water column. C includes the system specific parameters: initial laser power, the area of the receiving optics, the source divergence and the overlap function based on the field of view. The two optical parameters important to lidar returns are the angular scattering coefficient near 180° ( $\beta_{\pi}$ ) and lidar attenuation ( $\alpha$ ). Since this equation does not include multiple scattering it cannot account for increasing of the backscattered signal received by the detector at high turbidities. This can make the effective attenuation artificially small. The single scatter lidar equation thus has two unknowns. Techniques to incorporate multiple wavelengths<sup>4</sup> and multiple fields of view<sup>5</sup> show promise in strengthening retrievals of IOPs by providing analytical solutions to the lidar equation by decreasing the number of unknowns.

The omission of multiply scattered light is a complication for this form of the lidar equation. Attempts to quantify multiple scattering have been undertaken using Monte-Carlo<sup>6,7</sup> and Small Angle Approximation (SAA)<sup>8</sup>. These methods mostly require *a priori* information like the single scattering albedo and volume scattering function to achieve good performance. This is not entirely possible for an underwater autonomous system where there are stringent power and computational constraints. To alleviate this the multiple scattered light can be directly sampled using an off axis channel, which can look at a portion of the backscattered return outside the common volume. Through calibration using instrument specific algorithms it is possible to incorporate the multiply scattered signal without *a priori* knowledge and with relatively little computational effort.<sup>9</sup>

## 2. METHODS

A lidar system developed under NOAA-OAR funding was developed and is undergoing testing at Florida Atlantic University Harbor Branch Oceanographic Institute and is called OCULUS. The unit weighs approximately 37 pounds in air and has a small power draw. It is an eye safe system which includes both blue and green pulsed laser sources (473 and 532nm respectively). It is a bistatic lidar with a small separation between the receivers and source. It has two receivers, both with the same acceptance angle and distance from the source, but at different orientations with respect to the source. The off axis channels provide a greater view of the multiple scattered signal before the common volume<sup>9</sup>. The system has a vertical resolution of 5.625 cm. Each measurement is the average of at least 100 seconds of collection giving ten thousand scans for each measurement.

Table 1. Oculus lidar system specific parameters.

Wavelength (nm)	473	532
Pulse Energy ( $\mu$ J)	10	23.1
Pulse Duration (ns)	1.27	1.12
Pulse-Rep Rate (Hz)	100	
Beam Divergence (Deg)	1	
Ground Sample Dist (cm @ 1m/s)	1	
Vertical Resolution (cm)	5.625	

Testing was conducted in a purpose-built imaging tank facility with a blacked-out tank approximately 6.5x12.5x2 m. Approximately 60,000 black 2-inch spheres are placed on the surface of the tank for additional light rejection as well as to limit surface specular reflection. This method is 99% effective at light rejection. Jets on three of the four corners of the tank help to homogenize the particle population in the tank and limit settling. Barium sulfate and Arizona Road Test Dust (AZRD) were both employed as known particles in the test tank. Barium sulfate was selected due to its properties as a purely scattering particle whose absorption is negligible ( $b/c > 0.99$  (532nm)). Sodium hexametaphosphate was also included as an anticoagulant to prevent the barium sulfate from aggregating and settling out of the tank. AZRD, while having a large scattering component does absorb slightly more than barium sulfate ( $b/c = 0.85$ ). The concentration of particles was systematically controlled in the tank and increased to obtain an attenuation of 1.3 at roughly 0.1  $\text{m}^{-1}$  increments (at 532 nm). The phase function of both test particles was measured using the MASCOT (Multi-Angle Scattering Optical Tool)<sup>16</sup> and absorption and attenuation were measured using an ac-9<sup>17</sup>.



Figure 1. Image of Oculus Lidar inside the tank as it was deployed.

The lidar was mounted at the one end of the tank at midwater depth. A dark absorbing curtain was covering the other side. This helped to reduce specular reflection from the back wall. This has an added effect of filtering particles out of the water, so the turbidity cycles need to be conducted continuously and efficiently. All turbidity cycles were completed within 12 hours.

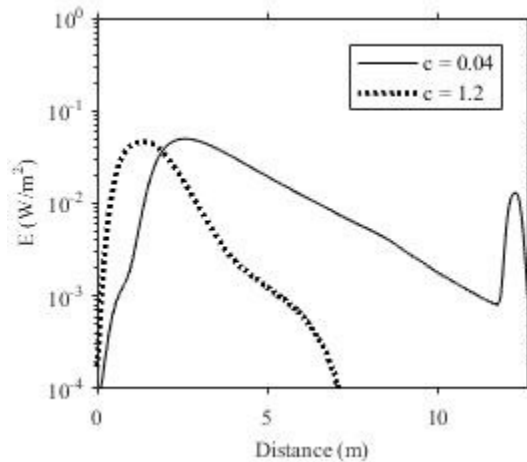


Figure 2. Example plot of lidar backscattered return as measured in the tank at a low and high turbidity.

Figure 1 shows the relative change in the backscattered lidar return from increasing turbidity. The two peaks on the  $c = 0.04$  plot are the beginning of the common volume and the backscattered return from the far wall of the tank. As  $c$  increases the initial peak moves closer to the receiver as multiple scattering takes more of a role in the signal, also more light is attenuated, increasing the slope. The common volume slope in a homogeneous system is generally proportional to a diffuse attenuation specific to the lidar geometry.

Determination of the slope needed to provide lidar diffuse attenuation  $\alpha$  requires a range correction first be applied. Range correction is required because lidar backscattered return decreases with distance by  $(1/r^2)$  as shown in the first equation. Range  $r = [v \Delta t/m]$  where  $v$  is the speed of light *in vacuo*. To accommodate this loss of signal the power returned at a given distance is corrected by multiplying the lidar backscattered return by  $r^2$ . The slope method can then be applied on the logarithmic transform of the corrected backscattered power for the range of the tank. A one-half multiplier considers the two way travel time of the photon. The final form of this equation is:

$$K_{sys} = \frac{1}{2} \frac{d}{dr} \ln[p(r)r^2]$$

This  $K_{\text{sys}}$  should fall between the downwelling extinction coefficient ( $K_d$ ) and the IOP beam attenuation  $c$ <sup>10,11,12</sup>.

Another technique used for short range determination of  $\alpha$  is to take the ratio of the integral of the multiple scattering signal (the signal before the common volume) and the integral of the common volume. This technique is relatively robust but can only be assumed to be valid close to the lidar and the common volume. This does not provide a range gated attenuation.

Using the Monte-Carlo backscatter module from Metron's Electro-Optic DETection Simulator (EODES), it is possible to test lidar geometries and configurations to determine their suitability for resolving the optical properties of a waterbody<sup>11,12</sup>. Measured IOP values allow validation of modeling efforts. After validation of the model with respect to each lidar system, permutations of inherent optical properties can be modeled and used to further characterize the lidar response. Another benefit of modeling this effect is the generation of a look up table for simpler and more robust inversion and analysis in real-time during deployments.

### 3. RESULTS

For the measured BaSO<sub>4</sub> and AZRD waveforms there was a slight increase of the lidar slope for the 2-4 m region. This effect increased as the turbidity of the tank was increased. This is likely due to effects of multiple scattering and the scattering phase function. The measured lidar returns had significantly greater slopes than the simulated returns at low turbidities. At higher turbidities the measured and simulated  $k_{\text{sys}}$  approached the same value for 473 nm. For 532 nm there was a consistent positive offset between the simulated and measured slopes. In all measured cases the slope of the lidar return was close but slightly larger than 1.

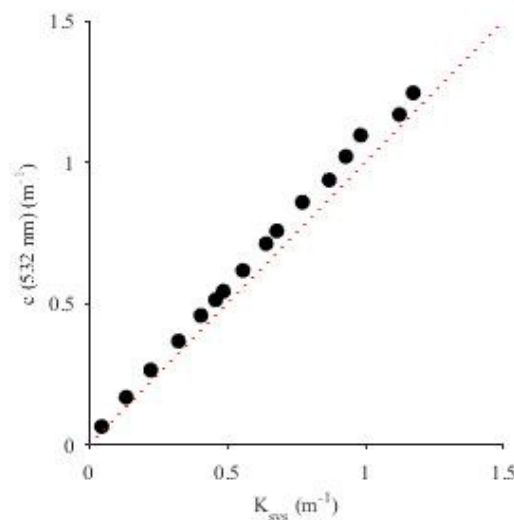


Figure 3. Relationship between measured attenuation with ac-9 and range corrected lidar slope, i.e.,  $K_{\text{sys}}$ , of simulated waveforms at 532 nm for BaSO<sub>4</sub>.

Comparison of model simulations of the barium sulfate with measurements from OCULUS, show strong linear relationships between  $k_{\text{sys}}$  values and  $c$ . Slopes for  $c$  vs  $k_{\text{sys}}$  were 1.02 and 1.4 for 532 and 473 nm respectively. There were also systematic offsets regarding the  $k_{\text{sys}}$  values. The strong linear relationships observed is strong evidence for the application of this lidar system to derive the IOP beam attenuation  $c$ . Deviations from an ideal 1:1 are thought to arise from a range correction requiring additional tuning, and from the different acceptance angles of the attenuation measurement from the ac-9 versus the OCULUS lidar system.

The AZRD produced similar results where the  $k_{\text{sys}}$  was also found to be higher than  $c$  for clear waters. As the turbidity increased however,  $k_{\text{sys}}/c$  values decreased to a value converging on 0.3. AZRD has a single scattering albedo of 0.85 on average at 532. Even with this high albedo it still behaves quite differently than the BaSO<sub>4</sub> due to a more forward peaked phase function. The system specific lidar slope did follow a linear relationship for this set of data as well.

Figure 3 shows the short-range determination of attenuation at 532 using the ratio of multiple scattered energy to the common volume energy for the simulated waveforms for barium sulfate. Both 532 and 473 showed very strong relationships. The form of the fit is a 3-parameter exponential equation ( $y = y_0 + a \cdot \exp(b \cdot x)$ ). Each wavelength did have a small intercept offset: 0.077 and 0.040 for 532 and 473 nm respectively and the  $a$  and  $b$  values are 0.062 and 4.04 for 532 and 0.071 and 4.01 for 473 nm.

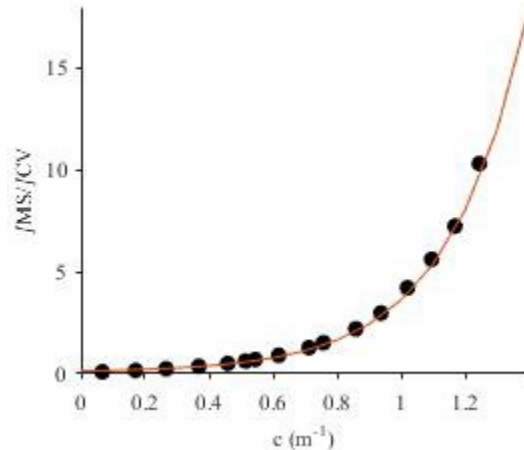


Figure 4. Ratio of the integral of the multiple scattering signal and the integral of the common volume.

#### 4. DISCUSSION

OCULUS lidar waveform slopes showed a strong linear relationship with beam attenuation  $c$ , indicating these measurements are readily amenable to inversion. Improving these relationships by adjusting the range correction and by accounting for the acceptance angle of the beam attenuation and lidar devices is required before a rigorous inversion algorithm can be developed for all water types.

Drawbacks of using the slope method lie with its sensitivity to small changes in homogeneity and the signal to noise ratio at far distances. No system is truly homogenous, and errors are amplified through use of the natural logarithm<sup>3</sup>. This basic method does not account for any multiple scattering. In the future several other techniques will be tested incorporating this systems' unique attributes and to maximize the retrieval of layers.

This system was in fact designed to be very sensitive to small changes in light so that it can best detect layers. Calibration of methods to account for the specific geometry of this lidar are paramount to the successful inversion of scattering returns. Much of the literature focuses around systems which have a source receiver separation that is negligible compared to the altitude above the water's surface which gives an almost complete overlap over the water. This system does have a narrow separation between the telescopes and the source, but this is larger than other systems. The initial portion of the lidar return is made up entirely of multiple scattering before the beginning of the common volume. This in combination with a direct measurement of multiple scattering with the off axis could help to determine the impact of multiple scattering to the lidar return. All these parameters can also be explored at both wavelengths of the system. The ideal wavelength for optimizing transmission in open waters is somewhere between 470 and 490 nm according to Gray et. al.<sup>4</sup> They also determined that green is useful for moderately turbid waters.

Many oceanographic lidar platforms are on aerial platforms.<sup>12</sup> these systems show strong dependence on their surface spot size<sup>10</sup>. Spot sizes for this type of system are quite large. The effective spot size of a profiling lidar will be significantly smaller than those examined by those in the aerial oceanographic lidar community<sup>11</sup>. This may explain how these values can be so close to 1 for inversion.

## 5. CONCLUSION

Future work will include field tests on and off AUVs, turbidity cycles in the test tank, and simulations. Other datasets including other test particles will help verify and validate the field efforts. Artificial thin layers will also be applied to the tank to generate test range gated inversion. Modeling will continue and will be tuned to match this specific system. The off-axis data will be inverted in the estimate of range-averaged beam  $c$  in the same range, leaving a quantitative means for correcting for the effects of multiple scattering. System specific calibrations will be applied to the empirical correction regime but will not require any previous knowledge of the VSF to estimate the  $c$  and MS contribution.

Thousands of unique optical situations will be modelled for the on and off axis receivers at both wavelengths and will be used to generate a look up table for this and other lidar systems. The use of the model provides a powerful testing ground for this and future systems and aids in the development of more robust algorithms and lidar systems.

The synthetic dataset which has been generated ranges between  $c$  values 0.04 and 12 at 532 nm logarithmically. At the extreme high end of the attenuation the lidar return is generally expected to be unusable, and therefore the range of chlorophyll values will be tuned for each system independently. This does however give rise to the question of how best to utilize the system's two wavelength component to maximize the efficacy of the system.

## 6. ACKNOWLEDGMENTS

This work was supported by the NOAA award NA140AR4320260 to the Cooperative Institute for Ocean Exploration, Research and Technology. The authors gratefully acknowledge support from the NOAA CIOERT at HBOI/FAU.

## REFERENCES

- [1] Morel, A., "Optical modeling of the upper ocean in relation to its biogenous matter content (case I waters)," *J. Geophys. Res.*, 93(C9), 10749–10768 (1988).
- [2] IOCCG, "Remote Sensing of Inherent Optical Properties: Fundamentals, Tests of Algorithms, and Applications, in Reports of the International Ocean-Colour Coordinating Group," No. 5, edited by Z.-P. Lee, p. 126, IOCCG, Dartmouth, Canada (2006)
- [3] Kovalev, V and Eichinger, [Elastic LiDAR. Theory, Practice and Analysis Methods], Wiley (2004)
- [4] Gray D., and Anderson J. E., Nelson J., Edwards J., "Using a multiwavelength LiDAR for improved remote sensing of natural waters," *Appl. Opt.* Vol. 54 No 31.232-242 (2015)
- [5] Feygels V. I., Kopilevich Y. I., Surkov A., Yungel J. K., and Behrenfeld M. J., "Airborne lidar system with variable field-of-view receiver for water optical properties measurement," *Proc. SPIE*, Vol. 5155, pp. 12-21, November 2003.
- [6] Kattawar GW, Plass GN. "Time of flight LiDAR measurements as an ocean probe," *Appl Opt.* 1972 Mar 1;11(3):662\_6.
- [7] Zege, E, Ivanov, A and Katsev, I. "Image Transfer through a scattering medium," Springer-Verlag, 1991.
- [8] Katsev, J, Zege E., Prikhach, A and Polansky, I. "Efficient Technique to determine backscattered light power for various atmospheric and oceanic sounding and imaging systems," *J. Opt. Soc. Am A.*, Vol14, N 6, 1997.
- [9] Vuorenkoski A. K., Dalglish F. R., Twardowski M. S., Ouyang B., Trees C. C., "Semi-empirical inversion technique for retrieval of quantitative attenuation profiles with underwater scanning lidar systems", *Proc. SPIE*, Vol. 9459, May 2015.
- [10] Howard R. Gordon, "Interpretation of airborne oceanic lidar: effects of multiple scattering," *Appl. Opt.* 21, 2996-3001 (1982)
- [11] Churnside, J.H. Review of Profiling Oceanographic LiDAR. *Optical Engineering* 53(5), 051405. (2014)
- [12] Ronald E. Walker and John W. McLean, "Lidar equations for turbid media with pulse stretching," *Appl. Opt.* 38, 2384-2397 (1999)
- [13] Giddings, T.E. and Shirron, J.J., Numerical Simulation of the Electro-Optical Imaging Process in Plane-Stratified Media, submitted to *Applied Optics*. (2008)
- [14] Dalglish, F., Vuorenkoski, A., Nootz, G., Ouyang, B., and Caimi, F., Experimental Study into the Performance Impact of the Environmental Noise on Undersea Pulsed Laser Serial Imagers. *U.S. Navy Journal of Underwater Acoustics*. Volume 61; Issue 4. (2011)

- [15] Twardowski, M.S., M. Lewis, A. Barnard, J.R.V. Zaneveld, "In-water instrumentation and platforms for ocean color remote sensing applications," In: Remote Sensing of Coastal Aquatic Waters, R. Miller, C. Del Castillo, and B. McKee [Eds.], Springer Publishing, Dordrecht, Netherlands, pp. 69-100 (2005).
- [16] Twardowski, M., X. Zhang, S. Vagle, J. Sullivan, S. Freeman, H. Czerski, Y. You, L. Bi, and G. Kattawar, "The optical volume scattering function in a surf zone inverted to derive sediment and bubble particle subpopulations," Journal of Geophysical Research, 117, C00H17, doi:10.1029/2011JC007347 (2012).
- [17] Twardowski, M.S., J.M. Sullivan, P.L. Donaghay, and J.R.V. Zaneveld, "Microscale quantification of the absorption by dissolved and particulate material in coastal waters with an ac-9," Journal of Atmospheric and Oceanic Technology, 16(12), 691-707 (1999).